eprints@whiterose.ac.uk
https://eprints.whiterose.ac.uk/

Optimal Design of Soft Continuum Magnetic Robots under Follow-the-leader Shape Forming Actuation

Peter Lloyd, Giovanni Pittiglio, James H. Chandler, Pietro Valdastri

Abstract— We describe a novel paradigm for task-specific optimization of millimetre scale, magnetically actuated soft continuum robots for application in endoscopic procedures. In particular, we focus on a multi-segment, elastomeric manipulator whose magnetization and actuating field is optimized for follow-the-leader shape forming during insertion into a known environment. Optimization of length-wise magnetization profile, or *magnetic signature*, is performed in parallel with that of the actuating magnetic field for a range of desired shapes. We employ a rigid-link model for the mechanics of the manipulator and assume the ability to generate a controlled homogeneous magnetic field across the workspace. To demonstrate the efficacy of the proposed approach, we present our results against those generated via Finite Element Analysis (FEA). Moreover, we compare our proposed method with a traditional tip-driven system exhibiting fixed magnetization; demonstrating a 48% error reduction in shape forming capability. The presented approach is evaluated across three additional navigation scenarios, demonstrating potential as a design tool for soft magnetic medical robots.

Index Terms— Steerable Catheters/Needles, Soft Material Robotics, Image-Guided Intervention.

I. INTRODUCTION

In the last few decades, much medical research and development has focused on minimally invasive diagnosis and treatment. We have seen the advent of technologies that can facilitate scare-less endoluminal inspection of the human body. In general this can improve patient outcomes through lower morbidity and reduced recovery times [1]. With the proliferation of minimally invasive procedures a number of technological challenges have arisen in relation to the tools involved. Specifically, there has been a need to reduce instrument size, increase dexterity, and improve safety during tissue interactions.

In summation, these challenges may be generally considered in relation to the tools' ability to effectively navigate through, and operate within, complex and tortuous environments. In pursuit of this capability researchers have extensively investigated the use of *continuum manipulators* [2]. These are generally characterised by high dexterity with some degree of shape control, making them highly suitable for application in minimally invasive diagnosis and treatment.

Although high dexterity is essential for navigation within complex environments, it is also important for safety and comfort to minimize inadvertent contact forces. For this reason, soft robots - with their elastomeric materials - have been proposed [3] and applied to surgical procedures [4]. A soft robot can rely on environmental interaction to provide shape forming forces without subjecting the patient to excessive discomfort or risk.

Enhanced shape forming of continuum robots, through higher controllable degrees of freedom, has the consequence of increasing their size. Indeed, across many actuation systems we can generally equate higher dexterity with a corresponding increase in size. An example of this, for tendon-driven manipulators, is the increase in number of tendons required as controlled degrees of freedom are increased [5]. Due to this restriction, much recent research has focused on *magnetically actuated* solutions [6], [7], [8]. In the case of magnetic actuation, dexterity is not directly correlated to size and miniaturization is no longer limited to very simple (one or two degree of freedom) shapes. Adversely, a corresponding relationship exists for magnets between maximum applicable force and their size. This can be counter-acted with the application of strong magnetic fields as in, for example, the Magnetic Resonance Imaging (MRI) fringe field detailed in [9].

As a consequence of the independence of size and dexterity, magnetic actuation has proven effective in endoscopic procedures [10], [11]. Single point [12], shape [13], multi-magnet [6], [7] and magnetic soft matter control [8] have all been investigated. One limitation of all of these approaches resides in sub-optimal magnetization profile - generally in the direction of motion - and focusing on magnetic field control only. This does not, in general, allow for minimized contact during navigation.

Inspired by [14], [15], [16], [17], [18], who demonstrate magnetic signature design for enhanced functionalities, we propose a novel procedure for optimal design of *magnetic soft tentacles* for endoscopic procedures. Starting from a known anatomical pathway, we optimize the tentacle magnetization along its length in conjunction with the instantaneous controlling magnetic field to minimize contact forces during insertion. An autonomous routine, based on a combination of rigid link [19] and magnetic modelling [20] has been designed to optimize the length-wise magnetization profile or *magnetic signature* of the tentacle. We consider the ten-

The authors are with the STORM Lab UK, School of Electronic and Electrical Engineering, University of Leeds, Leeds, UK. {men9prl, g.pittiglio, j.chandler, p.valdastri}@leeds.ac.uk.

tacle as being formed from multiple sections of magnetized elastomeric material operating under sequential insertion.

Following a detailed overview of the problem (Section II), we present the proposed optimization strategy including simplifying assumptions (Section III). The insertion process for the optimized multi-segment magnetic tentacle and controlling field is evaluated through implementation of rigid link and finite element simulations (Section IV). We assess our approach against a traditional tip-driven configuration, as well as verifying its efficacy over a range of navigation scenarios (Section V).

II. PROBLEM FORMULATION

Consider the problem of guiding a soft *tentacle* through a lumen, from an *insertion point* (I) to the *target point* (T) as depicted in Fig. 1. We assume the lumen shape is known from pre-imaging for example, and that the optimal (desired) path from I to T has been ascertained by means of either a manual or an automated path planning algorithm (e.g. [21]).

The aim in this case is to find the *magnetization* (μ_i) of the i-th link (L_i) and the global *homogeneous magnetic field* (B) such that the magnetized tentacle conforms to a desired shape, minimizing contact with the environment. This is achieved through an optimization procedure, detailed in Section III-C. The insertion process is considered to be step-wise; for each insertion step (δT) a new segment is introduced into the environment and its magnetization, along with the global homogeneous magnetic field $B(k\delta T)$, $k = 0, 1, \cdots$, is optimized to produce the desired shape.

In the present work we do not consider a specific actuation system, rather we assume a pure homogeneous field is generated throughout the work-space. This assumption is intuitively valid for the case of coil-based actuation [20] and can also be made for sufficiently small work-spaces (relative to magnets' remanence) in permanent magnet based counterparts such as [10].

To achieve suitable optimization, a model of the mechanical response of the tentacle as it interacts with its actuating magnetic field is required. Since we are dealing with a soft continuum robot, full mechanical characterization is not straightforward, and has been an active topic of research [22]. Here we employ the *rigid-link model* as already proposed for magnetically actuated continuum robots in [19].

III. MAGNETO-MECHANICAL DESIGN

In the following section, the modeling approach applied to the magnetic tentacle shown in Fig. 1 is described; including the mechanical and magnetic properties and their interaction. For the presented study, a planar case is considered, however, this could be generalised to more complex 3D scenarios.

A. Mechanics

Consider the insertion of a magnetically active tentacle starting from the insertion point (I) shown in Fig. 1. At each time step $t = k\,\delta T$, $k = 0, 1, \cdots$, we assume a segment of length δl is inserted into the environment. This process is assumed to be independent of the magnetic actuation, i.e.
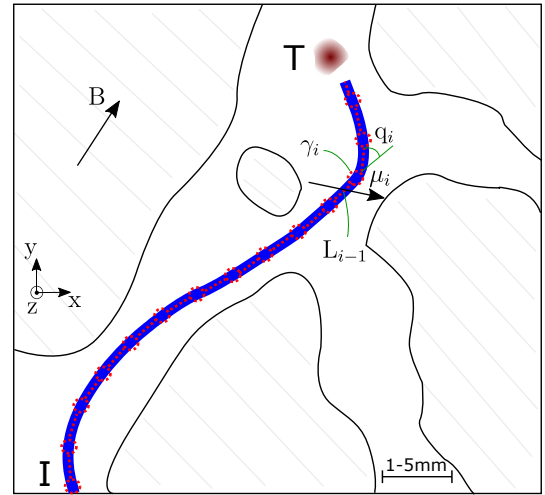
Fig. 1. Example of navigation of magnetic tentacle in generic lumen, from insertion point (I) to target point (T). Approximate scale bar shown to give indication of magnitude

the tentacle is mechanically introduced into the environment and not driven via magnetic wrenches. This segment will be the i-th link L_i of the continuum robot, connected to the link L_{i-1} and L_{i+1} by means of the *rotational joints* γ_{i-1} and γ_i, respectively.

The i-th joint angle q_i is defined as the angle between the link L_{i-1} and L_i, as per the standard Denavit-Hartenberg (DH) convention [23].

At the k-th insertion step, the robot joint space can be described by $q^{(k)} = (q_1 \ q_2 \ \cdots \ q_k)^T$. We consider that a wrench $f_j \in \mathbb{R}^6$ is applied at the centre of the j-th link whose end position is

$$p_j = -\sum_{i=1}^{j} \prod_{k=1}^{i} \text{rot}_z(q_k) \ \delta l \ e_2$$

where $\text{rot}_z(\cdot)$ is the rotation around the z axis and $e_r^{(s)} \in \mathbb{R}^s$ is the r-th element of the canonical basis of $\mathbb{R}^s$. For the sake of analytical simplicity we model components of the wrench which lie out of plane however these components do not play a role in the torque balance equation. Moreover, since we consider homogeneous magnetic field - hence, torque only - the location of the applied wrench along the link does not have effect on the results.

By considering the *differential kinematics* of the continuum manipulator [23], under the rigid-link assumption, the twist at the center of L_j can be expressed as

$$\begin{pmatrix} v_j \\ \dot{\theta}_j \end{pmatrix} = \sum_{i=1}^{j} \begin{pmatrix} (\frac{1}{2}p_j - p_i) \times \delta l \ e_3^{(3)} \\ e_3^{(3)} \end{pmatrix} \dot{q}_i = J_j^{(k)} \dot{Q}_k,$$

with θ_j deflection of the j-th segment and $v_j = \frac{\dot{p}_j}{2}$. By stacking the Jacobians for the j-th link at insertion step k, as $J^{(k)^T} = \begin{pmatrix} J_1^{(k)^T} & J_2^{(k)^T} & \cdots & J_k^{(k)^T} \end{pmatrix}$, and considering the duality between differential kinematics and statics, we obtain

$$\tau^{(k)} = J^{(k)^T} f^{(k)}, \tag{1}$$

with $f^{(k)} = (f_1^T \ f_2^T \ \cdots \ f_k^T)^T$ being the wrench applied to each inserted link. The torque on the joints $\tau^{(k)}$, considering

the tentacle's resting position $Q^{(k)} = 0_{k,0}$, with $0_{ij} \in \mathbb{R}^{i \times j}$ the zero vector, is

$$\tau^{(k)} = K^{(k)} Q^{(k)}, \tag{2}$$

where the stiffness matrix $K^{(k)}$ can be found from the mechanical characteristics of the material [19]. We assume, without loss of generality, that the stiffness is linear with respect to the joint variables. This assumption (which could be relaxed for the modelling of complex elastomeric behaviour and/or large deformation) is considered valid when δl is chosen to be *sufficiently small* and, thus, each q_i is small. Herein

$$K^{(k)} = \mathrm{diag}(\underbrace{EI \ EI \ \cdots \ EI}_{k \text{ times}}),$$

with E Young modulus and I second moment of area [24].

B. Magnetics

As introduced in Section II, we consider the i-th link of the tentacle to have magnetization μ_i, with respect to the link's reference frame. By considering the direct kinematics of the manipulator, in the global reference frame, we obtain

$$\overline{\mu}_i = \prod_{j=1}^{i} \mathrm{rot}_z(q_j) \mu_i.$$

In the case of our homogeneous field B, we obtain the wrench on the i-th link being [20]

$$f_i = \begin{pmatrix} 0_{3,1} \\ B \times \overline{\mu}_i \end{pmatrix} = \begin{pmatrix} 0_{3,1} \\ -\overline{\mu}_{i_\times} B \end{pmatrix},$$

with $(\cdot)_\times$ being the *skew operator*. We build the mapping from field to wrench as

$$S^{(k)} = \begin{pmatrix} 0_{3,3} \\ -\overline{\mu}_{k_\times} \\ 0_{3,3} \\ -\overline{\mu}_{k-1_\times} \\ \vdots \\ 0_{3,3} \\ -\overline{\mu}_{1_\times} \end{pmatrix}.$$

This, combined with (1) and (2), leads to the *magneto-mechanical static equilibrium*

$$K^{(k)} Q^{(k)} = J^{(k)^T} (S^{(k)} B(k\delta T) + G^{(k)}), \tag{3}$$

with the gravity vector $G^{(k)} = -mg^{(k)}$,

$$g^{(k)} = \left. \begin{pmatrix} e_2^{(6)} \\ e_2^{(6)} \\ \vdots \\ e_2^{(6)} \end{pmatrix} \right\} k \text{ times},$$

and m the mass of each link.

C. Optimization

The fundamental step of the proposed approach lies in the optimization of the magnetization $\mu = \left(\mu_1^T \ \mu_2^T \ \cdots \ \mu_n^T \right)^T$ and the magnetic field $U = \left(B(0) \ B(1) \ \cdots \ B((n-1)\delta T) \right)$. Herein, n is the number of segments needed to reach the target (T).

With this aim, we define the system of equations of the magneto-mechanical equilibrium

$$\lambda = \begin{pmatrix} K^{(1)} Q^{(1)} - J^{(1)^T} (S^{(1)} B(0) + G^{(1)}) \\ K^{(2)} Q^{(2)} - J^{(2)^T} (S^{(2)} B(\delta T) + G^{(2)}) \\ \vdots \\ K^{(n)} Q^{(n)} - J^{(n)^T} (S^{(n)} B((n-1)\delta T) + G^{(n)}) \end{pmatrix}$$

and the vector of unknowns $x = (\mu^T \ U^T)^T$. We thus solve the minimization problem

$$\min_x \quad ||\lambda||$$
$$\text{s.t.} \quad ||\mu_i|| = C, \ \forall i$$

by using the Matlab function `fmincon` [25], with the *interior point algorithm*.

Constraints are applied with consideration of fabrication simplicity. Specifically, we constrain the magnitude of magnetization to be constant in each segment representing a fixed proportion of magnetic doping throughout all magnetically active sections of the manipulator.

IV. NUMERICAL ANALYSIS

In order to assess the strength of the proposed approach we performed a Finite Element Analysis (FEA) representing four distinct scenarios; different configurations of obstacles in a planar environment. We considered a desired path (Γ_d) connecting the insertion point with the target point - the origin and the green circle respectively in Figs. 2, 3, 4, 5, 6. The sample path was generated considering four segments of equal length $\delta l = 14mm$. This length gives sufficient flexibility to exhibit length-wise shape forming without being so flexible as to violate the assumptions of linear elasticity; we noticed breakdown in the validity of the rigid link assumption for $q_i > 15^o$.

The algorithm described in Section III was applied to determine the case-specific magnetization (μ_i for the i-th segment) and the magnetic field at each time step (B). In parallel to our rigid-link model (see Section III-A), a full continuum mechanics FEA model was constructed using the commercial software package COMSOL multiphysics v5.4 (COMSOL AB, Stockholm, Sweden). This simulation employed the solid mechanics and electro-magnetics modules connected via the Maxwell surface stress tensor. The plane strain assumption was utilised and the 78,000 node manually assembled mesh was converged using the Newton-Raphson iterative method.

The tentacle radius was fixed at 1 mm. Each of the four identical 14 mm long segments was assembled in series from 7 mm of magnetically unreactive silicone (Ecoflex 00-30, Young Modulus 69 kPa, density 1070 kgm^{-3}) and 7
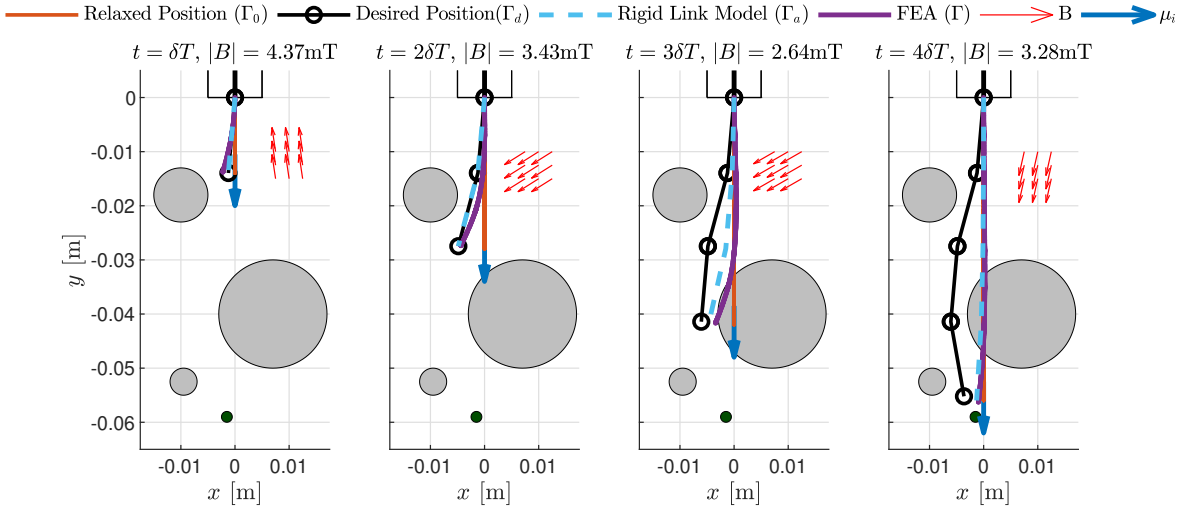
Fig. 2. Scenario A*. The tip driven catheter with optimized magnetic field showing collision at $t = 4\delta T$
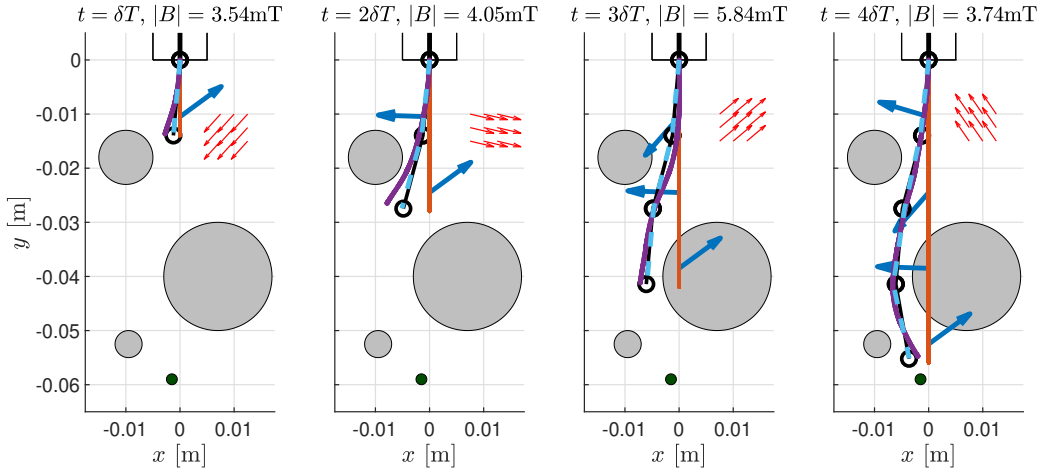
Fig. 3. Scenario A. The fully shape forming tentacle shown successfully navigating an identical environment to Scenario A*. For legend see Fig. 2.

TABLE I

A COMPARISON OF RMS ERRORS (mm) FOR THE TIP DRIVEN CATHETER (A*) AND THE FULLY MAGNETIZED TENTACLE IN FOUR DIFFERENT TOPOLOGICAL SCENARIOS (A, B, C AND D). ROW 3 ALSO SHOWS THE ABSOLUTE ERROR IN FINAL TIP POSITION (mm)

	Scenario A*		Scenario A		Scenario B		Scenario C		Scenario D	
	$\Gamma_d - \Gamma$	$\Gamma_d - \Gamma_a$	$\Gamma_d - \Gamma$	$\Gamma_d - \Gamma_a$	$\Gamma_d - \Gamma$	$\Gamma_d - \Gamma_a$	$\Gamma_d - \Gamma$	$\Gamma_d - \Gamma_a$	$\Gamma_d - \Gamma$	$\Gamma_d - \Gamma_a$
Tip Deflection	**2.0**	1.4	**2.0**	0.14	4.3	0.10	4.0	0.38	2.2	0.02
Full-shape Deflection	**2.5**	1.97	**1.3**	0.19	2.2	0.17	3.1	0.23	1.2	0.03
Final Tip Position	**2.7**	2.34	**1.7**	0.04	6.6	0.10	6.4	0.16	2.3	0.01

mm of magnetically reactive silicone (Young Modulus 80 kPa, density 1400 kgm^{-3}, remanent magnetization 107 mT). These properties were calculated assuming equal proportions by weight of silicone and Neodymium-iron-boron (NdFeb) in the doped segments of the tentacle [8]. Notice that, even if the rigid-link model used in the optimization does not, the COMSOL simulation considers magnetic interaction between reactive segments. This numerical simulation provides a series of derived tentacle shapes (Γ) which we assumed to be an accurate representation of reality. The Young modulus and density of the arbitrary homogenised

material represented by the rigid link model are weighted means of those in the numerical model.

V. RESULTS

In order to compare the performance of the rigid link optimization with previously proposed techniques applied to magnetically actuated soft continuum robots [8] we established a basis for comparison. This comparison is made for the first arrangement of obstacles only; Scenario A* versus Scenario A. To this end, an initial scenario (Scenario A*) was considered with a fully constrained magnetization representing a conventional tip driven continuum manipulator;
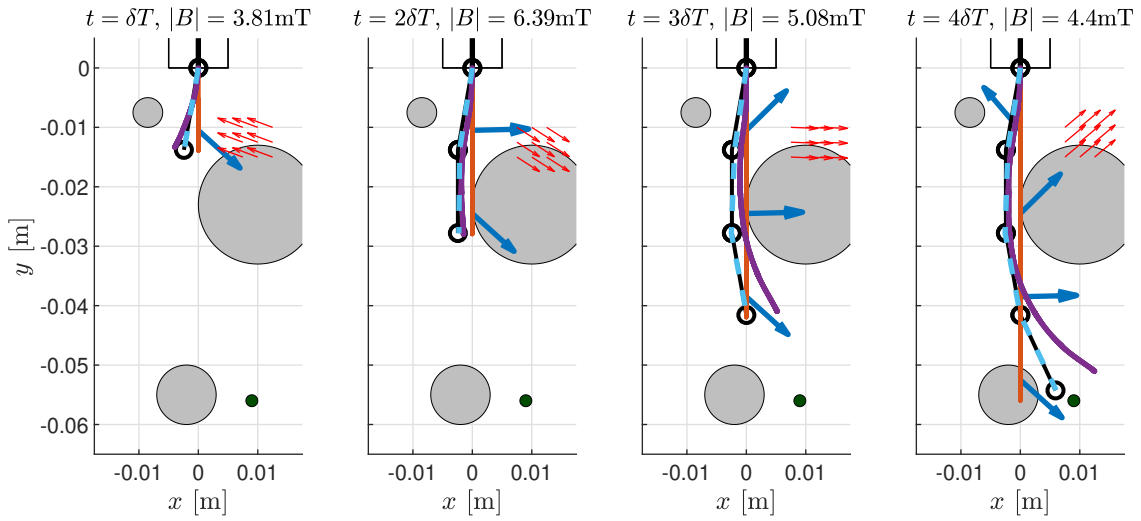
Fig. 4. Scenario B. An alternative arrangement of obstacles
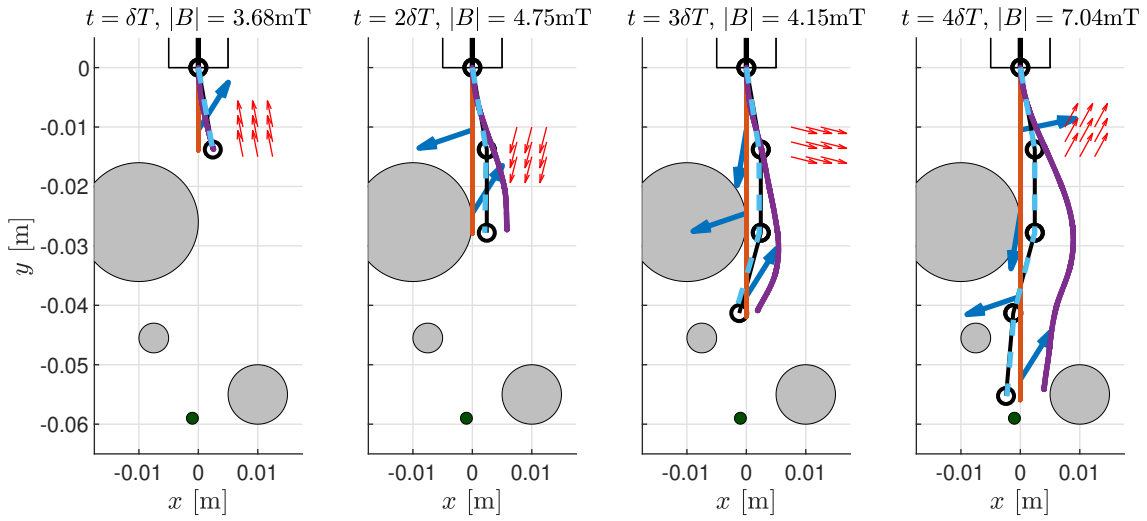
Fig. 5. Scenario C. The constraint of a homogeneous field appears prohibitive for this more convoluted path
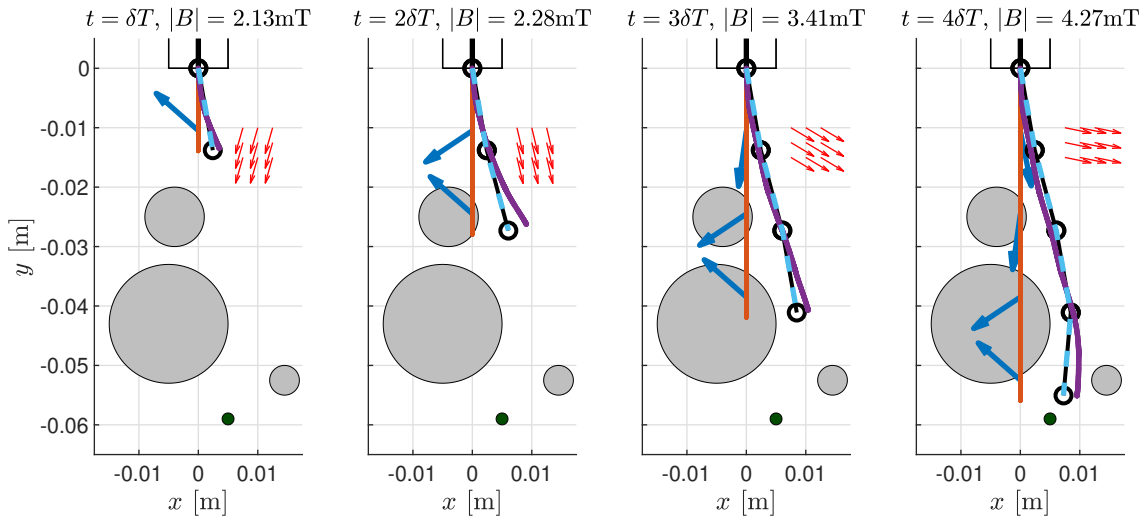
Fig. 6. Scenario D. A fourth arrangement of obstacles demonstrating a high level of reconciliation between rigid link and FEA models

optimized for field only. This is reported in Fig. 2 where the impact with an interstitial obstacle (the grey circles in, for example, Fig. 2) can be clearly observed. This approach would therefore rely on environmental interaction to navigate such a pathway, as shown in [8]. Conversely, as detailed in Fig. 3, the proposed method, by design, eliminates contact and demonstrates obstacle avoidance.

To demonstrate the diversity of the proposed methodology, we presented three further cases of successful obstacle avoidance in Figs. 4, 5 and 6. All four of the evaluated scenarios successfully avoid collision. however Scenario C (Fig. 5), due to its more convoluted desired shape exhibits errors in magnitude of deflection. The requested profile in Scenario C changes direction mid-length and as a consequence of this complication the rigid link optimization fails to produce an accurate replica of the FEA. Whilst the deflected shape is produced, accuracy is lost in the magnitude of deflection. This is due to the constraint of a homogeneous field; were field gradients and their associated forces permitted, the optimization may more accurately replicate this more convoluted desired shape.

Table I reports the Root Mean Square (RMS) of errors in deflection in the x axis between the desired path and the FEA result (Left hand sub-column; $\Gamma_d - \Gamma$) and between the desired path and the rigid link model result (Right hand sub-column; $\Gamma_d - \Gamma_a$). Errors are presented for each of the five scenarios in Figs 2, 3, 4, 5 and 6 respectively. The first of these Scenarios (A*) being the purely tip driven example and the subsequent four scenarios being our fully shape forming analyses with various obstacle locations.

Errors for each of these five illustrated scenarios are presented in three distinct forms represented by the rows of Table I. In row 1 the error in the position of *just* the tip is shown, the average is taken of the tip position at each of the four insertion time-steps

$$\epsilon = \sqrt{\frac{1}{T}\sum_{t=1}^{T}(p_{x,d}^{(t)} - p_x^{(t)})^2}$$

with $p_{x,d}^{(t)}$ *desired* x position of the tip at time t, $p_x^{(t)}$ the same for *derived* value and T the total number of time steps.

In row 2 we show the error in the position of *all* of the segment centres at every time step

$$\epsilon = \sqrt{\frac{1}{NT}\sum_{t=1}^{T}\sum_{i=1}^{N}(p_{x,d}^{(i,t)} - p_x^{(i,t)})^2}$$

with $p_{x,d}^{(i,t)}$ *desired* x position of the i-th segment at time t, $p_x^{(i,t)}$ the same for *derived* value and N the total number of segments. This second row provides a suitable proxy for the error in the shape forming capability of the tentacle. Finally, in row 3 we show the absolute error (in mm) of the finishing tip position.

From this we can make an objective comparison of the tip driven example in Scenario A* against our shape forming

example in Scenario A. This comparison is shown in bold-face in Table I. We can see that the error in the tip position does not improve when a full length-wise magnetization is employed. For the full body shape error in row 2, however, an error reduction of 48% is shown. This reduction is intuitively apparent, as the tip driven system has no capacity to shape form as is observable in Fig. 2. For the shape forming tentacle, across all four topographies we observe an RMS error between desired and derived segment positions of 2.1mm (3.7% of manipulator length) with a standard deviation of 0.9mm (1.6% of manipulator length).

Further to this, across all four shape forming Scenarios (Figs. 3, 4, 5 and 6) it is observed that the rigid link model exhibits very close adherence to the desired shape. This level of accuracy is not replicated when the results of the rigid link model are processed in the FEA. From this we conclude that there remain inaccuracies in the assumptions of the rigid link model which are exposed by the FEA. These inaccuracies most notably relate to link length and the linear pseudo-spring constant. We intend to address and minimize these in our future work.

VI. CONCLUSIONS

In this work we described a novel approach for the parallel optimization of magnetic signature and actuating field for our soft continuum magnetized manipulators or *magnetic tentacles*. We focused on the problem of minimizing interaction with the environment and hence increasing patient safety and comfort. The proposed approach relies on magneto-mechanical modelling of the static equilibrium of the continuum manipulator. This system is based on a combination of magnetic dipole and rigid-link mechanical models. By considering this equilibrium, we performed an off-line optimization procedure which outputs the optimal magnetization profile of the tentacle and the attendant actuating fields at each step of insertion. We defined the application as a planar case under the assumption that a homogeneous magnetic field can be generated across the work-space.

We reported numerical results from the FEA for four different obstacles settings. We also computed the comparison, for the first of these settings, of non-optimized magnetization - the tip driven manipulator. This resembles previously proposed approaches in the literature [7], [9], [8]. We showed that the proposed solution achieves significantly improved results in terms of follow-the-leader path following accuracy and obstacle avoidance.

Our future work will be devolved to improvements and developments in the rigid link modelling assumptions, applying the proposed method to a 3D case and investigating cases of non-homogeneous magnetic field. Moreover, we will analyse and report experimental studies.

References

[1] K. A. Hausegger, P. Schedlbauer, H. A. Deutschmann, and K. Tiesenhausen, "Complications in endoluminal repair of abdominal aortic aneurysms," *European journal of radiology*, vol. 39, no. 1, pp. 22–33, 2001.

[2] J. Burgner-Kahrs, D. C. Rucker, and H. Choset, "Continuum Robots for Medical Applications: A Survey," pp. 1261–1280, 12 2015.

[3] D. Trivedi, C. D. Rahn, W. M. Kier, and I. D. Walker, "Soft robotics: Biological inspiration, state of the art, and future research," *Applied Bionics and Biomechanics*, vol. 5, no. 3, pp. 99–117, 2008.

[4] M. C. Yip, J. A. Sganga, and D. B. Camarillo, "Autonomous Control of Continuum Robot Manipulators for Complex Cardiac Ablation Tasks," *Journal of Medical Robotics Research*, vol. 02, no. 01, p. 1750002, 2017.

[5] T. Kato, I. Okumura, H. Kose, K. Takagi, and N. Hata, "Tendon-driven continuum robot for neuroendoscopy: validation of extended kinematic mapping for hysteresis operation," *International Journal of Computer Assisted Radiology and Surgery*, vol. 11, no. 4, pp. 589–602, 4 2016.

[6] J. Edelmann, A. J. Petruska, and B. J. Nelson, "Magnetic control of continuum devices," *International Journal of Robotics Research*, vol. 36, no. 1, pp. 68–85, 2017.

[7] S. Jeon, A. K. Hoshiar, K. Kim, S. Lee, E. Kim, S. Lee, J.-y. Kim, B. J. Nelson, H.-J. Cha, B.-J. Yi, and H. Choi, "A Magnetically Controlled Soft Microrobot Steering a Guidewire in a Three-Dimensional Phantom Vascular Network," *Soft Robotics*, vol. 6, no. 1, pp. 54–68, 10 2018. [Online]. Available: https://doi.org/10.1089/soro.2018.0019

[8] Y. Kim, G. A. Parada, S. Liu, and X. Zhao, "Ferromagnetic soft continuum robots," *Science Robotics*, vol. 4, no. 33, p. eaax7329, 8 2019. [Online]. Available: http://robotics.sciencemag.org/content/4/33/eaax7329.abstract

[9] A. Azizi, C. C. Tremblay, K. Gagné, and S. Martel, "Using the fringe field of a clinical MRI scanner enables robotic navigation of tethered instruments in deeper vascular regions," *Science Robotics*, vol. 4, no. 36, p. eaax7342, 11 2019. [Online]. Available: http://robotics.sciencemag.org/content/4/36/eaax7342.abstract

[10] L. Barducci, G. Pittiglio, J. C. Norton, K. L. Obstein, and P. Valdastri, "Adaptive Dynamic Control for Magnetically Actuated Medical Robots," *IEEE Robotics and Automation Letters*, vol. 4, no. 4, pp. 3633–3640, 7 2019.

[11] J. C. Norton, P. R. Slawinski, H. S. Lay, J. W. Martin, B. F. Cox, G. Cummins, M. P. Y. Desmulliez, R. E. Clutton, K. L. Obstein, and S. Cochran, "Intelligent magnetic manipulation for gastrointestinal ultrasound," *Science Robotics*, 2019.

[12] G. Pittiglio, L. Barducci, J. W. Martin, J. C. Norton, C. A. Avizzano, K. L. Obstein, and P. Valdastri, "Magnetic Levitation for Soft-Tethered Capsule Colonoscopy Actuated With a Single Permanent Magnet: A Dynamic Control Approach," *IEEE Robotics and Automation Letters*, vol. 4, no. 2, pp. 1224–1231, 2019.

[13] L. B. Kratchman, T. L. Bruns, J. J. Abbott, and R. J. Webster, "Guiding Elastic Rods With a Robot-Manipulated Magnet for Medical Applications," *IEEE Transactions on Robotics*, vol. 33, no. 1, pp. 227–233, 2017.

[14] S. Floyd, C. Pawashe, and M. Sitti, "An untethered magnetically actuated micro-robot capable of motion on arbitrary surfaces," in *2008 IEEE International Conference on Robotics and Automation*, 2008, pp. 419–424.

[15] W. Hu, G. Z. Lum, M. Mastrangeli, and M. Sitti, "Small-scale soft-bodied robot with multimodal locomotion," *Nature*, vol. 554, p. 81, 1 2018. [Online]. Available: https://doi.org/10.1038/nature25443http://10.0.4.14/nature25443https://www.nature.com/articles/nature25443#supplementary-information

[16] G. Z. Lum, Z. Ye, X. Dong, H. Marvi, O. Erin, W. Hu, and M. Sitti, "Shape-programmable magnetic soft matter," *Proceedings of the National Academy of Sciences*, vol. 113, no. 41, pp. E6007 LP – E6015, 10 2016. [Online]. Available: http://www.pnas.org/content/113/41/E6007.abstract

[17] Y. Kim, H. Yuk, R. Zhao, S. A. Chester, and X. Zhao, "Printing ferromagnetic domains for untethered fast-transforming soft materials," *Nature*, vol. 558, no. 7709, pp. 274–279, 2018. [Online]. Available: https://doi.org/10.1038/s41586-018-0185-0

[18] R. Zhao, Y. Kim, S. A. Chester, P. Sharma, and X. Zhao, "Mechanics of hard-magnetic soft materials," *Journal of the Mechanics and Physics of Solids*, vol. 124, pp. 244–263, 2019. [Online]. Available: http://www.sciencedirect.com/science/article/pii/S0022509618307646

[19] V. K. Venkiteswaran, J. Sikorski, and S. Misra, "Shape and contact force estimation of continuum manipulators using pseudo rigid body models," *Mechanism and Machine Theory*, vol. 139, pp. 34–45, 2019.

[20] S. Salmanipour and E. Diller, "Eight-Degrees-of-Freedom Remote Actuation of Small Magnetic Mechanisms," in *2018 IEEE International Conference on Robotics and Automation (ICRA)*, 2018, pp. 3608–3613.

[21] C. Baykal, C. Bowen, and R. Alterovitz, "Asymptotically optimal kinematic design of robots using motion planning," *Autonomous Robots*, vol. 43, no. 2, pp. 345–357, Feb 2019. [Online]. Available: https://doi.org/10.1007/s10514-018-9766-x

[22] R. J. Webster and B. A. Jones, "Design and kinematic modeling of constant curvature continuum robots: A review," *International Journal of Robotics Research*, vol. 29, no. 13, pp. 1661–1683, 2010.

[23] B. Siciliano, L. Sciavicco, L. Villani, and G. Oriolo, *Robotics: Modelling, Planning and Control*. Springer Publishing Company, Incorporated, 2010.

[24] D. C. Rucker and R. J. I. Webster, "Statics and Dynamics of Continuum Robots With General Tendon Routing and External Loading," *IEEE Transactions on Robotics*, vol. 27, no. 6, pp. 1033–1044, 2011.

[25] "Matlab optimization toolbox," version R2018b, the MathWorks, Natick, MA, USA.